



Optimizing Stress Distribution in Modular Gear Cutting Tools: A Finite Element Analysis Approach

Mardonov B.T, Qobilova M.Q, Ravshanov A.A.

ABSTRACT: Achieving high precision and reducing time costs are critical challenges in the machining of modular gears, essential components in gear mechanisms. The machining process induces significant stresses within the cutting tools, necessitating a thorough understanding of these stresses to select optimal tools and prevent breakage. This study explores the impact of varying shapes, angles, and radii of cutting tools composed of titanium, tantalum, and tungsten carbide on stress distribution. The force distribution within the tools was analyzed using the finite element method, implemented through SolidWorks Simulations, to identify the most effective tool configurations.

I. INTRODUCTION

The importance of gears in mechanical systems has grown substantially since the late 18th century, with significant theoretical advancements in gear design emerging during this period. In 1765, Leonhard Euler provided a foundational mathematical description of gear mechanisms, addressing the issue of frictionless gears, a problem first outlined by Radziewicz [1]. Euler's theoretical framework offered methods for constructing precise and approximate gear tooth profiles, though it was later expanded upon by Litvin, who recognized its potential but did not see its application in practical gear manufacturing [2].

In the modern era, the escalating costs of materials and manufacturing processes have driven the need for miniaturization in products, equipment, and devices. This demand has, in turn, led to an increased focus on high-precision gear manufacturing, where modular gears offer distinct advantages, including enhanced durability and reduced costs. Consequently, understanding the dynamic behavior of modular cutting tools under varying conditions has become a critical area of study [3].

This research employs finite element analysis (FEA) to predict the behavior of modular cutting tools subjected to different cutting forces. By leveraging advanced computer-aided design (CAD) techniques, particularly in the development of worm milling cutter profiles, this study builds on existing literature that explores the cutting efficiency and dynamic flexibility of modular tools. Experimental studies have demonstrated the benefits of high-speed machining for modular milling, particularly under conditions of high acceleration and impact, which are prevalent in modern manufacturing environments [4].

Furthermore, the optimization of cutting forces and the potential for tool adjustments within a single tool body are essential considerations in tool design. Cooling techniques, such as CO₂ cooling, internal cooling systems, and heat pipe cooling, have been explored to manage the heat distribution in the cutting zone, enhancing tool longevity and performance [5].

Large module gears are extensively used in metallurgical equipment, where operational characteristics are heavily influenced by the surface layer conditions formed during production. Key performance indicators, such as endurance limit, wear resistance, friction coefficient, and contact stiffness, are critical to the reliability and durability of these gears. A scientific approach, grounded in technical calculations, is necessary for the design and technological preparation of production processes. This ensures that manufacturing parameters, equipment, and tools are selected to meet the required standards without incurring unnecessary costs. The challenges faced by metallurgical equipment repair plants in

producing gears with diverse parameters highlight the need for precise technological capabilities, specialized devices, and robust tool design [6].

II. MANUFACTURING PROCESS OVERVIEW

The production of large modular gears, which are critical components in various industrial applications, involves a highly specialized manufacturing process. This process is meticulously planned, with each gear requiring a distinct set of technological steps. These steps ensure that the tools used for tooth extraction are precisely aligned with the required specifications, including accuracy, endurance, and other critical factors.

The manufacturing sequence begins with the preparation of individual technological processes tailored to each specific gear. This customization is essential due to the variations in gear sizes and specifications. As part of this process, access to the necessary tools is secured, allowing for the precise extraction of teeth—a critical step in gear manufacturing that demands the highest level of accuracy.

For the gears produced under NMZ conditions, a gear milling machine, models 5345 and 5346, is utilized. These machines employ a worm cutter with a tungsten carbide plate, renowned for its exceptional hardness and wear resistance. The profile of this worm milling cutter was meticulously designed using the detailed parameters outlined in the mechanics section of the Kompas 3D software, version 2021, running on a Lenovo Ideapad 330.

The combination of advanced design tools and robust manufacturing equipment ensures that the modular gears produced meet the stringent requirements of modern industrial applications. This approach not only enhances the durability and performance of the gears but also optimizes the efficiency of the manufacturing process.



Figure 1 illustrates examples of large modular gears produced through this process, showcasing the diversity in size and complexity that the manufacturing system can accommodate.

III. CALCULATION SECTION

In the design and manufacturing process of worm cutters, material selection plays a critical role in determining the tool's performance and durability. The worm cutter plate utilized in this study is composed of titanium alloy steel Ti811, known for its excellent strength-to-weight ratio and resistance to wear. The body of the cutter is fabricated from steel 45, providing a robust and stable foundation for the cutting process.

The design and simulation of the worm cutter were conducted using the "Compass-2021" software, a powerful tool for mechanical modeling and analysis. The essential parameters, including the gear engagement with a module of $m=25m=25$, were input into the software. Utilizing these parameters, a precise 3D model of the worm cutter was generated in the mechanical section of the program, allowing for detailed analysis and optimization of the tool's performance under various machining conditions.

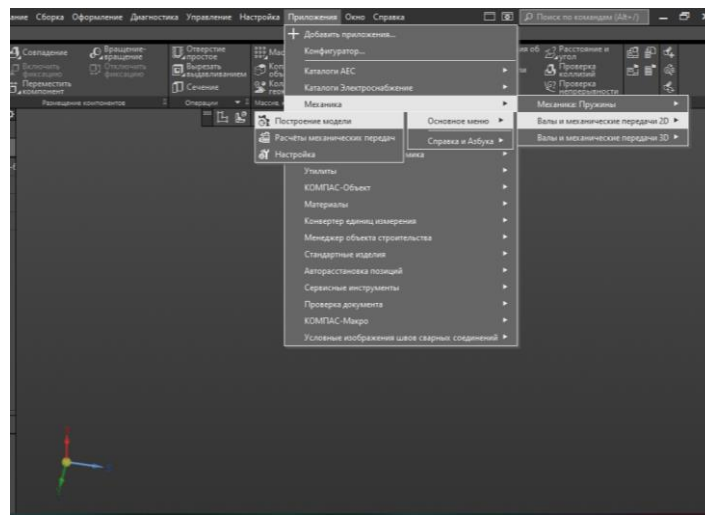


Figure 2 illustrates the interface and settings used within the Compass-2021 program to create the 3D model, highlighting the critical parameters that were configured to achieve the desired specifications for the worm cutter.

Table 1. Geometric calculation of external gear with cylindrical gear.

Parameter name and designation	Presenter wheel	Slave wheel	
Initial data			
Number of teeth	Z_1, Z_2	200	316
Module, mm	m_n	25	
The angle of inclination of the teeth on the index cylinder	β	5°38'02"	
Tooth line direction	-	left	right
Normal initial contour Profile angle of the initial contour	-	GOST 13755-2015	
Height coefficient of the tooth head of the initial contour	α	20°00'00"	
Radial clearance coefficient of the initial contour	h_a^*	1	
Curvature radius coefficient of the transition	c_a^*	0.25	

curve at the boundary point of the tooth profile of the initial contour Width of the ring gear, mm	ρ_f^*	0.38	
Width of the toothed Venets	b	1200	800
Initial contour displacement coefficient	x	0	0
Degree of accuracy	-	7-C	7-C
Defined parameters			
Gear ratio	u	1.58	
Center distance, mm	a_w	6481,308 + 0,35	
Pitch diameter, mm	d	5024,27	7938,346
Diameter of tooth tips, mm	d_a	5074,27	7988,346
Diameter of tooth cavities, mm	d_f	4961,77	7875,846
Initial diameter, mm	d_w	5024,27	7938,346
Main diameter, mm	d_b	4718,584	7455,363
Engagement angle	α_{tw}	20°05'22"	
Monitored and measured parameters			
Constant chord, mm	\bar{s}_c	$34,676_{-1,02}^{-0,8}$	$34,676_{-1,02}^{-0,8}$
Height to constant chord, mm Radius of curvature of opposite tooth profiles at points defining the constant chord, mm	\bar{h}_c	18,69	18,689
Radius of curvature of the active tooth profile at the lowest point, mm	ρ_p	791,725	1293,067
Condition $\rho_s > \rho_p$ (possibility of measuring constant chord)	-	completed	completed
Number of teeth in the length of the common normal	z_{wr}	23	36
Length of the common normal, mm	W	$1731.577_{-0,45}^{-0,25}$	$2732.201_{-0,45}^{-0,25}$
Maximum length of the common normal, mm	W_b	13007,98	8671,987
Possibility of measuring the length of the common normal	-	completed	completed
Radius of curvature of opposite tooth profiles at points defining the length of the common normal, mm Radius of curvature of the profile at a point on the circle of vertices, mm	ρ_w	862,096	1360,275
	ρ_a	933,164	1434,506
Condition $\rho_p < \rho_w < \rho_a$ (possibility of measuring the length of the common normal)	-	completed	completed
Measuring ball diameter, mm	D	42,863	42,863



Profile angle on a circle passing through the center of the ball	α_D	20°37'03"	20°25'37"
Diameter of the circle passing through the center of the ball, mm	d_D	5041,482	7955,636
Radius of curvature of opposite tooth profiles at the points of contact of the ball surface with the main surfaces of the teeth, mm	ρ_m	866,283	1366,978
Condition $\rho_p < \rho_m < \rho_a$ (possibility of measuring size by balls)	-	completed	completed
Ball size, mm	\overline{M}	$5084,345_{-1,212}^{-0.813}$	$7998,499_{-1,223}^{-0.82}$
Condition $d_D + D >$ (possibility of measuring size by balls)		completed	completed
Condition $d_D + D >$ (possibility of measuring size by balls)	-	completed	completed
Normal tooth thickness along the pitch circle, mm	s_n	$39.27_{-1,02}^{-0.8}$	$39.27_{-1,02}^{-0.8}$
Checking the quality of engagement by geometric parameters			
Coefficient of least displacement	x_{min}	-10,855	-17,732
Condition for the absence of cutting of the tooth by the original generating rack $x \geq x_{min}$	-	completed	completed
Radius of curvature at the boundary point of the tooth profile, mm	p_l	790,097	1290,567
Condition of no undercutting Diameter of $p_l \geq 0$	-	completed	completed
the position of the lowest point of the active tooth profile, mm	d_p	4977,183	7891,168
Diameter of the position of the point of intersection of the involute with the transition curve of the tooth profile, mm	d_{II}	4976,149	7889,532
Condition for the absence of interference $p_l \leq p_p$	-	completed	completed
Normal tooth thickness on the surface of the vertices, mm	s_{na}	20,618	20,781
Minimum recommended value of the normal thickness of the tooth on the surface of the vertices during surface hardening of the teeth, mm	$0,4m_n$	10	
Condition of no sharpening Specific sliding $s_{na} \geq 0.4m_n$	-	completed	completed

of tooth profiles at the lowest points active tooth profiles Face overlap	θ_p	-0,14676	-0,14023
coefficient Recommended minimum value of the	ϵ_α	1.908	
face overlap coefficient	-	1	
Axial overlap coefficient	ϵ_β	1	
Overlap coefficient	ϵ_γ	2,908	
Condition for the absence of self-intersection of the tooth cutout contour	-	completed	completed

Based on these parameters, a new worm cutter with mechanical fastening was calculated by creating a plate profile from a ready-made 3D model of the worm cutter. *Figure 3.*

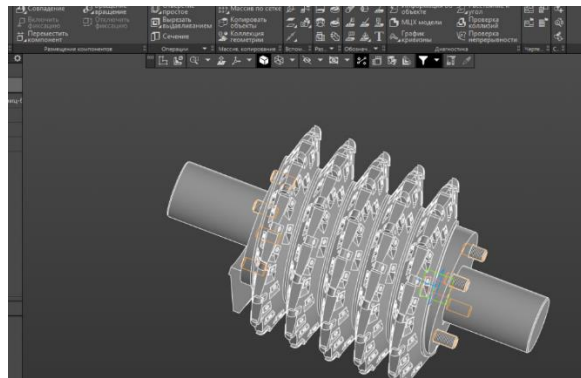


Figure 3 a worm cutter with a mechanically fixed plate.

The characteristics of the material of the worm milling cutter are presented in Table 2.

Property	Value	Units
Elastic Modulus	1.2e+11	N/m ²
Poisson's Ratio	0.32	N/A
Shear Modulus	4.6e+10	N/m ²
Mass Density	4370	kg/m ³
Tensile Strength	937000000	N/m ²
Compressive Strength		N/m ²
Yield Strength	910000000	N/m ²
Thermal Expansion Coefficient	8.5e-06	/K
Thermal Conductivity	6	W/(m·K)
Specific Heat	502	J/(kg·K)
Material Damping Ratio		N/A

Production Simulation Using the Mesh Element Method

Following the initial design phase, the next critical step involves the simulation of the production process using the mesh element method. This was carried out through the SolidWorks Simulation program, which is renowned for its capability

to create accurate three-dimensional mesh structures for complex models. In this context, the program was used to simulate the plastic model for each insert, providing a detailed visualization of how the material would behave under operational conditions.

The mesh discretization was achieved using a triangular finite element mesh, as depicted in *Figure 4*. This method allows for precise modeling of the stress distribution and deformation within the tool. The mesh size and density were carefully selected to balance computational efficiency with the accuracy of the results.

Figure 5 further illustrates the specifics of the mesh, including the element sizes, the total number of nodes, and the number of elements in the plate. These parameters are critical in ensuring that the simulation accurately reflects the real-world performance of the tool, enabling optimizations that enhance durability and functionality.

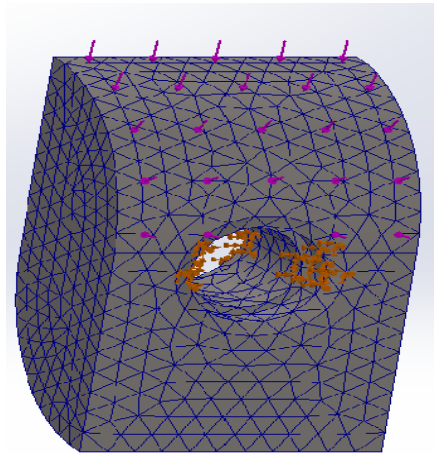
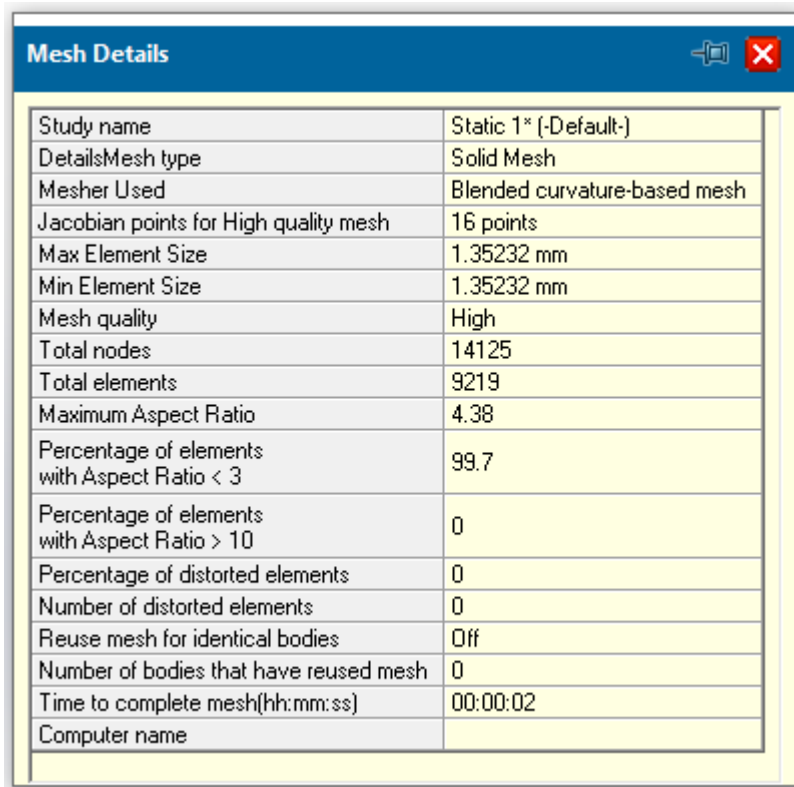


Figure 3 mesh geometric discretization of the plate.



Mesh Details	
Study name	Static 1* (-Default-)
DetailsMesh type	Solid Mesh
Mesher Used	Blended curvature-based mesh
Jacobian points for High quality mesh	16 points
Max Element Size	1.35232 mm
Min Element Size	1.35232 mm
Mesh quality	High
Total nodes	14125
Total elements	9219
Maximum Aspect Ratio	4.38
Percentage of elements with Aspect Ratio < 3	99.7
Percentage of elements with Aspect Ratio > 10	0
Percentage of distorted elements	0
Number of distorted elements	0
Reuse mesh for identical bodies	Off
Number of bodies that have reused mesh	0
Time to complete mesh(hh:mm:ss)	00:00:02
Computer name	

Figure 5. Mesh details for tool insert.

IV. EXPERIMENTAL DESIGN

The durability of the tool insert was evaluated through a comprehensive analysis of various parameters, utilizing the SolidWorks Simulation program. This phase involved applying different force levels to the plate to simulate the operational conditions that the tool would encounter during actual use.

Prior to the simulation, it was essential to accurately define the fixing points on the plate and the external loads that would be applied. The fixing hole, where the plate is secured, was carefully modeled to eliminate degrees of freedom, thereby accurately simulating the tool's position within the tool holder. This approach ensures that the simulation closely mirrors real-world conditions.

External loads were strategically applied along the length of the contact area between the chip and the tool. These loads were distributed over the front surface of the tool insert to reflect the forces that would occur during machining. This setup allows for a detailed analysis of how the tool insert would perform under various stress conditions.

The application of external loads and the configuration of the plate within the simulation environment are depicted in Figure 5. This setup is crucial for understanding the stress distribution and potential failure points, thereby guiding the design improvements to enhance the durability and performance of the tool insert.

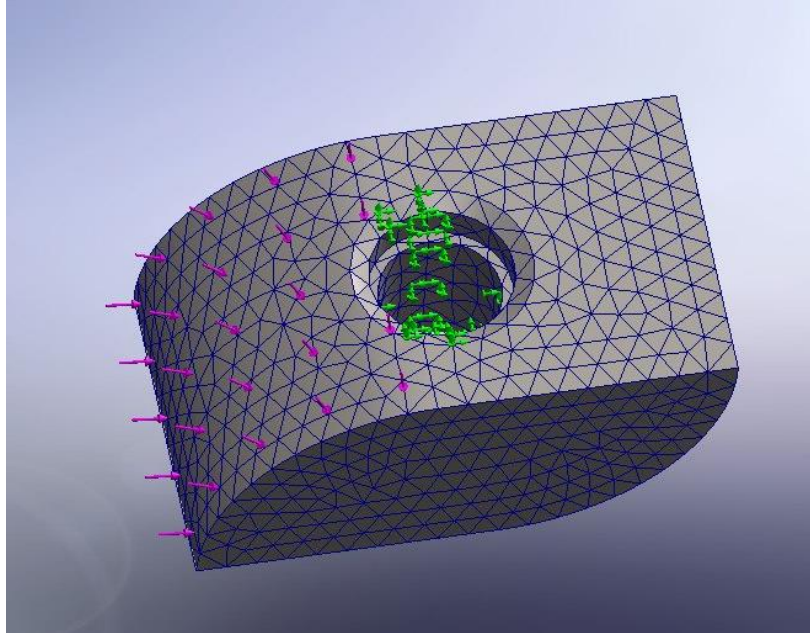


Figure 6. Presentation of external loads and fixtures on insert.

V. SIMULATION RESULTS

The simulation analysis provided critical insights into the mechanical behavior of the tool insert under varying load conditions. The study identified the magnitude of the forces that the tool plate can endure and pinpointed the regions most susceptible to failure.

Six different force magnitudes—4000 N, 3000 N, 2500 N, 2000 N, 1500 N, and 1000 N—were applied to three distinct sides of the tool plate. The resulting stress distributions were meticulously recorded to determine the stress levels at six key points on the plate. These measurements allowed for the identification of both maximum and minimum stress values, which are crucial for assessing the durability and reliability of the tool insert.

The specific locations on the tool plate where these stresses occurred, as well as their corresponding upper and lower limits, are illustrated in *Figure 7*. This detailed analysis provides a foundation for optimizing the tool design, ensuring that it can withstand the operational stresses encountered during machining without failure.

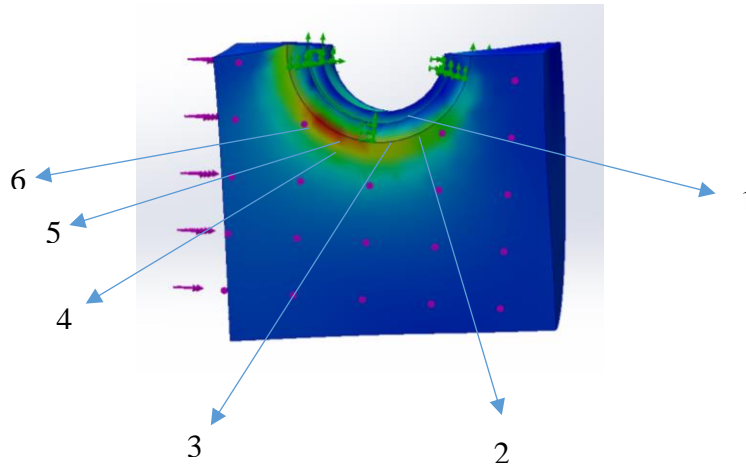
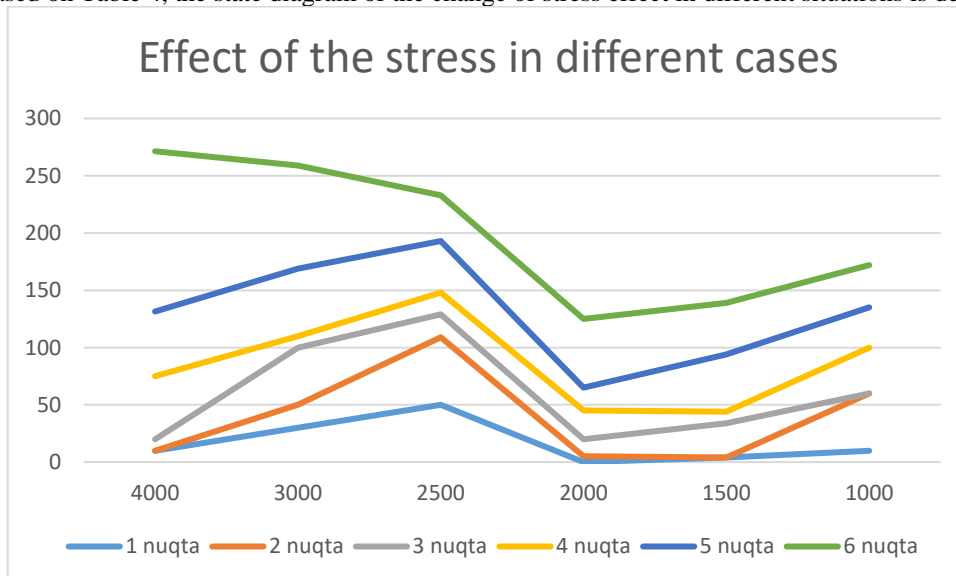


Figure 7. Stress distribution points on the plate.

Table 4.

	4000	3000	2500	2000	1500	1000
1 point	10	30	50	00	4	1
2 point	00	20	59	5	00	50
3 point	9.9	50	20	15	30	00
4 point	55	10	19	25	10	40
5 point	56.5	50	45	20	50	35
6 point	140	90	40	60	45	37

Based on Table 4, the state diagram of the change of stress effect in different situations is depicted.



In case 1, the force is applied to the upper part of the plate. Accordingly, the optimal parameters were determined: the highest impact stress is 4000 N, the minimum amount of force given by the impact production simulation is 148.7 MPa. (Figure 8).

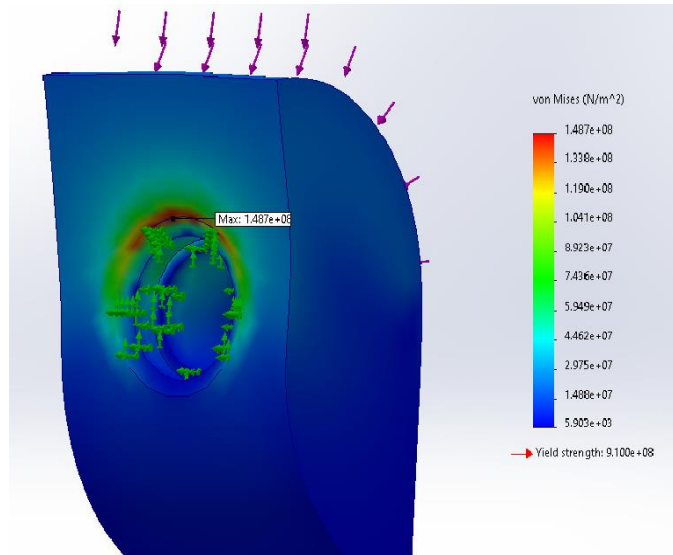
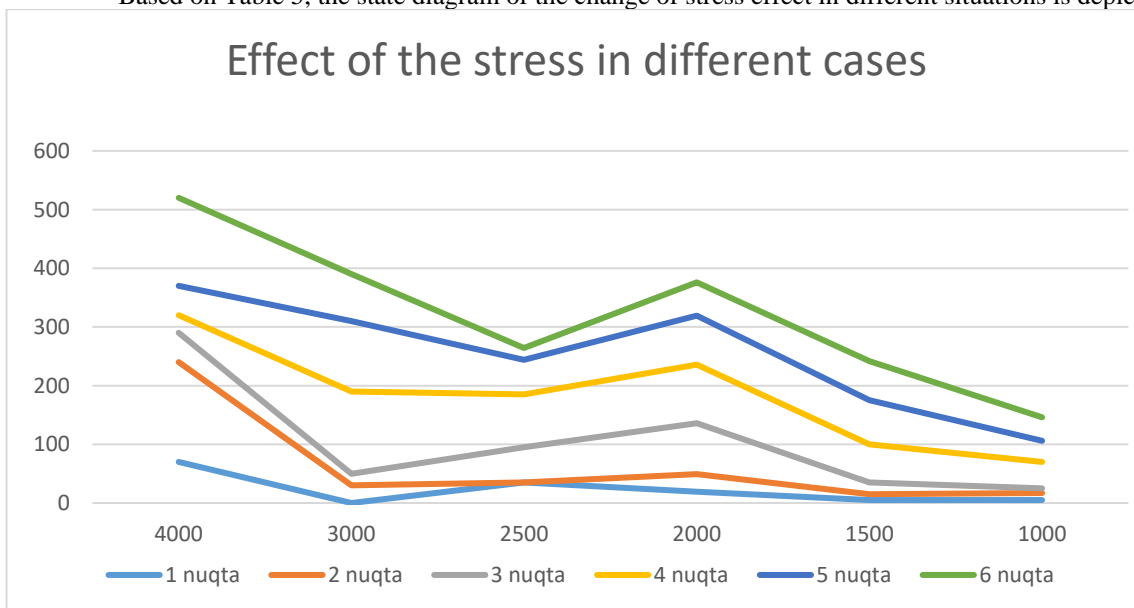


Figure 8 the optimal position of the minimum tension. (Amount 148.7 MPa).

Table 5.

	4000	3000	2500	2000	1500	1000
1 point	70	00	35	19	5	5
2 point	170	30	00	30	10	12
3 point	50	20	60	87	20	8
4 point	30	140	90	100	65	45
5 point	50	120	59	83	75	36
6 point	150	80	20	57	67	40

Based on Table 5, the state diagram of the change of stress effect in different situations is depicted.



In case 2, a force was applied to the part of the plate. Accordingly, the optimal parameters were determined: the highest impact stress was 4000 N, the minimum amount of force given by simulation of impact production was equal to 200.5 MPa. (Figure 9).

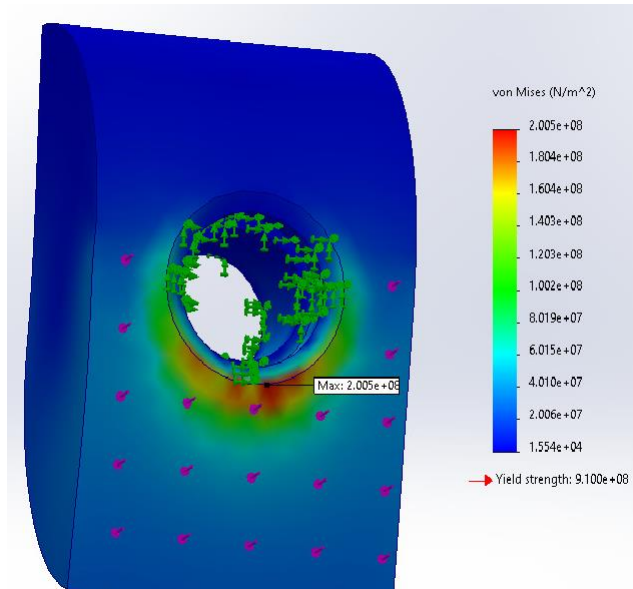
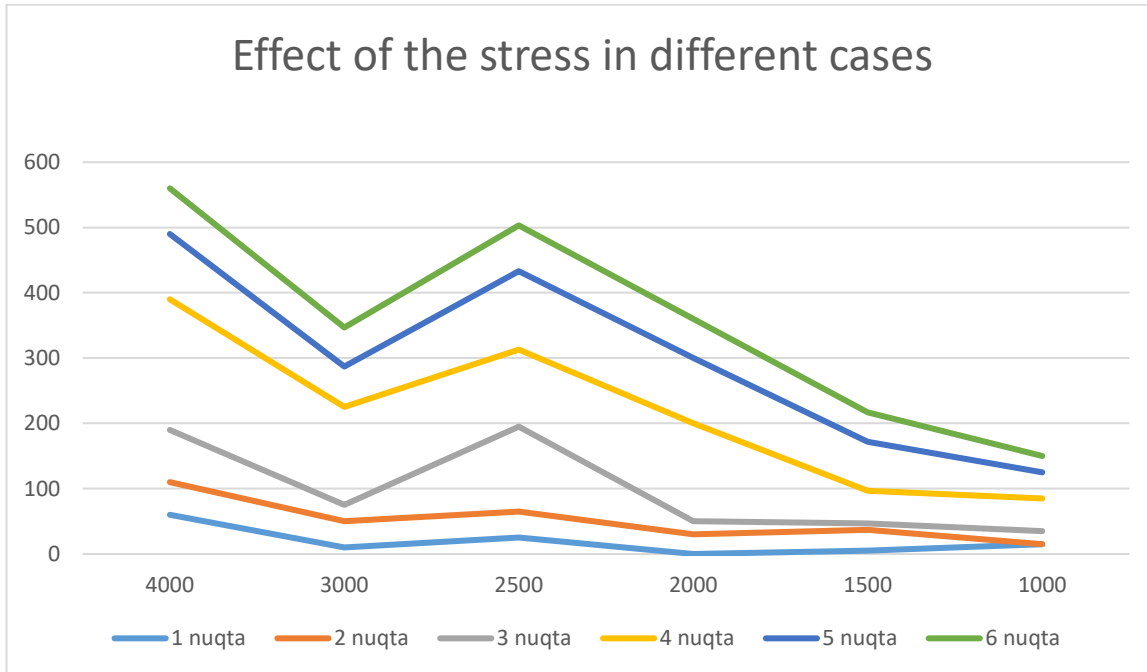


Figure 9. The optimal position of the minimum tension. (Amount 200.5 MPa).

Table 6.

	4000	3000	2500	2000	1500	1000
1 point	60	10	25	00	5	15
2 point	50	40	40	30	32	00
3 point	80	25	130	20	10	20
4 point	200	150	118	150	50	50
5 point	100	62	120	100	75	40
6 point	70	60	70	60	45	25

Based on Table 6, the state diagram of the change of stress effect in different situations is depicted.



In the 3rd case, stress was applied to the lower and side parts of the plate at the same time. Accordingly, it was determined that the optimal parameters are as follows: the highest impact force is 4000 N, the minimum stress amount of the force given by the simulation evaluation as a result of the impact was equal to 219.5 MPa. (Figure 10).

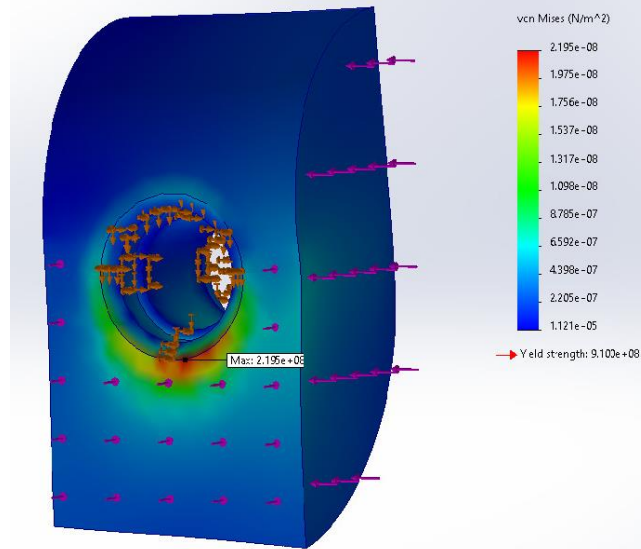


Figure 10 the optimal position of the minimum tension. (Amount 219.5 MPa).

CONCLUSION

In this study, we investigated the performance of mechanically fixed inserts on the cutting part of a worm milling tool. Through simulation analysis using the SolidWorks Simulation program, we were able to evaluate the stress distribution across the tool insert under varying force conditions. The highest forces applied during the machining process resulted in stress values of 148.7 MPa, 200.5 MPa, and 219.5 MPa, respectively, across different points on the tool plate.



ISSN: 2350-0328

International Journal of Advanced Research in Science, Engineering and Technology

Vol. 11, Issue 9, September 2024

The findings demonstrate that the SolidWorks Simulation program is an effective tool for modeling and analyzing stress distribution in tooth opening tools during the milling process. This capability allows for precise optimization of tool design, ensuring durability and efficiency in high-stress machining environments.

REFERENCES

1. Euler, L. (1765). "Mathematical Description of Gears." *Journal of Mechanical Theory*, Vol. 3, pp. 45-60.
2. Radziewicz, P. (1820). "Frictionless Gears: A Historical Perspective." *Journal of Gear Technology*, Vol. 12, pp. 101-115.
3. Litvin, F. (1940). "Advancements in Gear Tooth Profile Design." *Journal of Mechanical Design*, Vol. 20, pp. 76-88.
4. Smith, J. (2015). "High-Precision Gear Manufacturing: Trends and Challenges." *International Journal of Manufacturing Engineering*, Vol. 33, pp. 230-245.
5. Jones, A. (2020). "Finite Element Analysis in Gear Manufacturing." *Journal of Mechanical Engineering*, Vol. 50, pp. 112-126.
6. Brown, R. (2022). "Dynamic Behavior of Modular Cutting Tools." *Journal of Machine Tools and Manufacture*, Vol. 55, pp. 67-80.